

ornl

ORNL/TM-13197

RECEIVED

SEP 09 1986

OSTI

**OAK RIDGE
NATIONAL
LABORATORY**

LOCKHEED MARTIN 

Investigation of a Noncontact Strain Measurement Technique

B. Damiano
L. J. Talarico

MASTER

MANAGED AND OPERATED BY
LOCKHEED MARTIN ENERGY RESEARCH CORPORATION
FOR THE UNITED STATES
DEPARTMENT OF ENERGY

ORNL-27 (3-96)

DISTRIBUTION OF THIS DOCUMENT IS UNLIMITED

RB

This report has been reproduced directly from the best available copy.

Available to DOE and DOE contractors from the Office of Scientific and Technical Information, P. O. Box 62, Oak Ridge, TN 37831; prices available from (423) 576-8401, FTS 626-8401.

Available to the public from the National Technical Information Service, U.S. Department of Commerce, 5285 Port Royal Road, Springfield, VA 22161.

This report was prepared as an account of work sponsored by an agency of the United States Government. Neither the United States Government nor any agency thereof, nor any of their employees, makes any warranty, express or implied, or assumes any legal liability or responsibility for the accuracy, completeness, or usefulness of any information, apparatus, product, or process disclosed, or represents that its use would not infringe privately owned rights. Reference herein to any specific commercial product, process, or service by trade name, trademark, manufacturer, or otherwise, does not necessarily constitute or imply its endorsement, recommendation, or favoring by the United States Government or any agency thereof. The views and opinions of authors expressed herein do not necessarily state or reflect those of the United States Government of any agency thereof.

**INVESTIGATION OF A NONCONTACT STRAIN
MEASUREMENT TECHNIQUE**

B. Damiano
Instrumentation and Controls Division

L. J. Talarico
Engineering Technology Division

Date Published—May 1996

Research sponsored by the Laboratory Directed Research Program of Oak Ridge National Laboratory.

Prepared by
OAK RIDGE NATIONAL LABORATORY
Oak Ridge, Tennessee 37831-6285
managed by
LOCKHEED MARTIN ENERGY RESEARCH CORP.
for the
U.S. DEPARTMENT OF ENERGY
under contract DE-AC05-96OR22464



DISCLAIMER

**Portions of this document may be illegible
in electronic image products. Images are
produced from the best available original
document.**



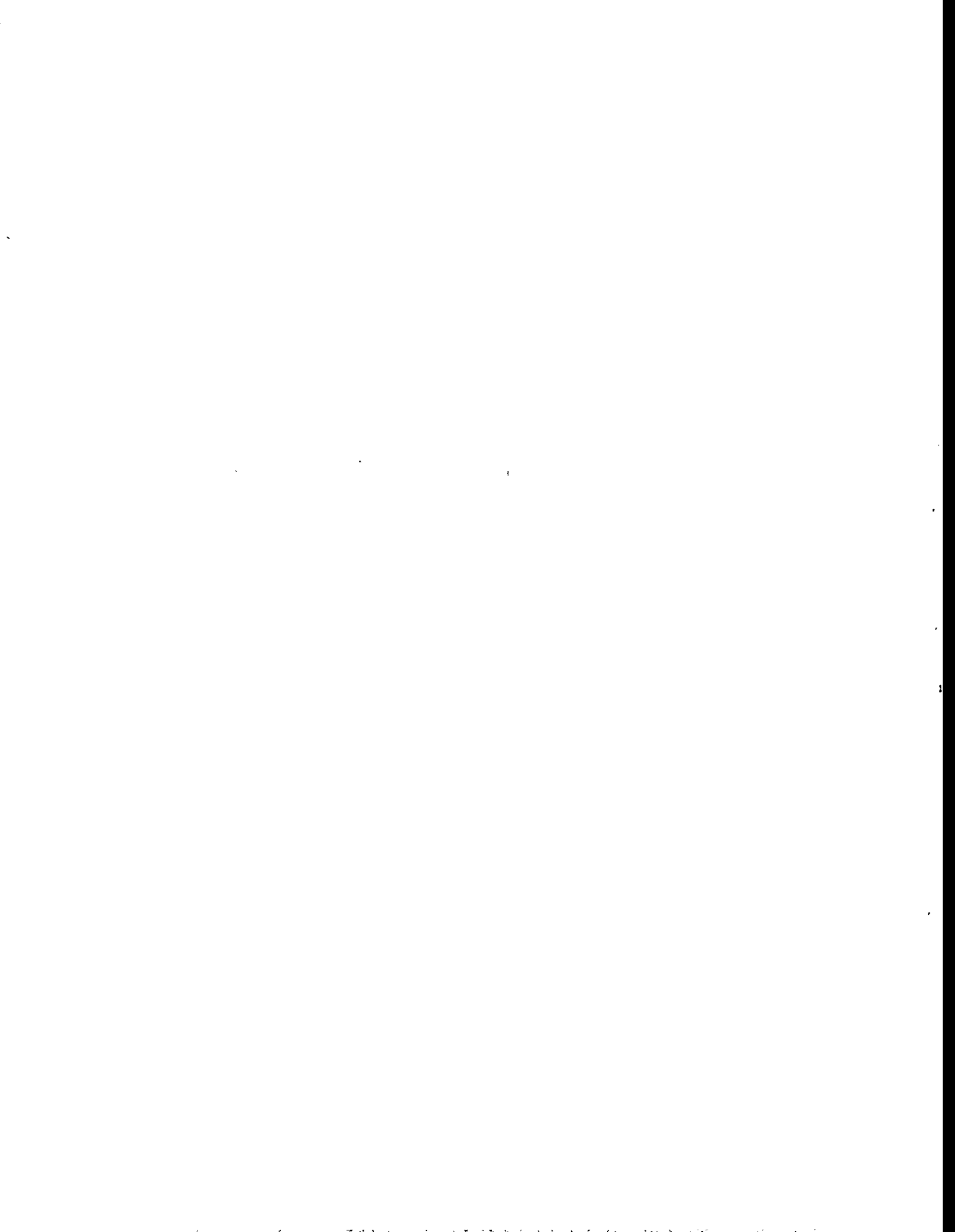
CONTENTS

LIST OF FIGURES	v
LIST OF TABLES	vii
ABSTRACT	ix
1. INTRODUCTION	1
2. FINITE ELEMENT MODEL AND PARAMETRIC STUDY DESCRIPTION	2
3. CALCULATION RESULTS	8
3.1 AXISYMMETRIC MAGNETOSTATIC RESULTS	8
3.2 TWO-DIMENSIONAL MAGNETOSTATIC AND NONLINEAR TRANSIENT RESULTS	8
4. CONCLUSIONS AND RECOMMENDATIONS	8
5. REFERENCES	12
APPENDIX A: MAGNETIC MATERIAL PROPERTIES	13



LIST OF FIGURES

Figure		Page
1	A typical application of a TRIP steel sensor to measure strain in a rotating component	2
2	The finite element model	3
3	B-H curves used in the analysis for TRIP steel	5
4	Flux density for 100% strained TRIP steel with a 2.54-mm air gap	6
5	Magnetic flux perturbation caused by the presence of 100% strained TRIP steel with a 2.54-mm air gap	7
6	Magnetic flux density averaged over the inner pole face for strain levels ranging from 0% to 100% and air gaps of 2.54, 12.7, and 25.4 mm	9
7	Magnetic flux density averaged over the pole face for strain levels ranging from 50% to 100%; TRIP steel disk velocities of 0, 2.54, 12.7, and 25.4 m/s; and an air gap of 2.54 mm	10
8	Magnetic flux density averaged over the pole face for strain levels ranging om 10% to 100%; TRIP steel disk velocities of 0, 2.54, 12.7, and 25.4 m/s; and an air gap of 12.7 mm	10
9	Magnetic flux density averaged over the pole face for strain levels ranging from 10% to 100%; TRIP steel disk velocities of 0, 2.54, 12.7, and 25.4 m/s; and an air gap of 25.4 mm	11
10	Magnetic flux density averaged over the pole face for strain levels ranging from 10% to 100% and air gaps of 2.54, 12.7, and 25.4 mm	11



LIST OF TABLES

Table		Page
1	Effect of TRIP steel strain and air gap on average inner pole flux density	9
A.1	Magnetic material properties	13
A.2	B-H data for electrical steel	14
A.3	B-H data for TRIP steel	15

ABSTRACT

The goal of this project was to investigate the feasibility of a new noncontact technique for directly and continuously monitoring peak strain in rotating components. The technique utilizes the unique strain-sensitive magnetic material properties of *TRansformation Induced Plasticity* (TRIP) steel alloys to measure strain. These alloys are weakly magnetic when unstrained but become strongly ferromagnetic after mechanical deformation. A computer study was performed to determine whether the strain-induced change in the magnetic material properties of a TRIP steel gage bonded to a rotating component would cause significant perturbations in the magnetic flux of a stationary electromagnet. The effects of strain level, distance between the rotating component and the stationary electromagnet, and motion-induced eddy currents on flux perturbation magnitude were investigated.

The calculated results indicate that a TRIP steel strain sensing element can cause a significant perturbation in the magnetic flux of a stationary electromagnet. The magnetic flux perturbation magnitude was found to be inversely proportional to the distance between the magnet face and the TRIP steel element and directly proportional to the TRIP steel strain level. The effect of motion-induced eddy currents on the magnetic flux was found to be negligible. It appears that the technique can be successfully applied to measure peak strain in rotating components; however, the sensitivity of the magnetic flux perturbation magnitude to the distance between the strain sensing element and the electromagnet may require making an independent proximity measurement.



1. INTRODUCTION

The project described in this report investigated a new technique for directly and continuously monitoring peak strain in rotating components. In current techniques for monitoring the structural condition of rotating components, an indirect indication of structural degradation, such as abnormal noise because of excessive vibration, is used, or a direct indication obtained by examining the rotating component during shutdown is used. Although failure of rotating components is relatively rare because of conservative design and intense maintenance and inspection programs, occasional failures can have severe economic or safety consequences. A recent example of steam turbine blade failure at the Fermi-2 nuclear plant on December 25, 1993, is estimated to have cost Detroit Edison in excess of \$35 million.¹ Continuous monitoring of rotating components could possibly eliminate some of the currently performed maintenance and inspection procedures while increasing the reliability of these components.

The technique combines the use of a TRIP (*TR*ansformation *I*nduced *P*lasticity)² steel strain sensing element attached to the rotating component, a stationary magnetic coil to provide a magnetic field, and a stationary magnetic field sensor to measure changes in the magnetic field caused by magnetic property changes in the strain sensing element. In this technique the metastable structure of TRIP steel is used to measure maximum strain. TRIP steels are initially in a metastable austenitic face-centered cubic phase. When subjected to deformation, the crystal structure changes to a martensitic body-centered tetragonal phase, with the amount of material undergoing the phase change being proportional to the peak strain.² The martensitic phase is ferromagnetic, while the austenitic phase is paramagnetic; thus the magnetic properties can be used to determine the prior peak strain a part has experienced. TRIP steel sensors have been applied to measure strain in stationary components such as bridge members and for structural mining applications.³ The innovative aspects of this project are the extension of this application to rotating components and the use of TRIP steel sensors to perform continuous strain monitoring.

The TRIP steel sensing elements are used to indicate high strain levels in rotating components in the following way (Fig. 1):

1. Attach the TRIP steel strain sensing element to the rotating component at the location where peak strains or failure are known or are predicted to occur. The sensing element may be a strip located inside the rotating component or a foil bonded to the surface.
2. Mount a stationary magnetic coil so that the magnetic field produced will interact with the TRIP steel strain sensing element during part of the component's rotation.
3. Mount a stationary magnetic field sensor, such as a Hall effect probe, to measure the coil's magnetic field strength.

Initially, with the strain sensing elements unstrained, the magnetic field sensor should detect little or no change in the coil's magnetic field when the strain sensing element is within the region occupied by the magnetic field. As the strain sensing elements deform, making the strain sensing element more ferromagnetic, it is anticipated that magnetic field perturbations will occur when the strain sensing element passes through the magnetic field. These perturbations should be measurable for sufficiently large strains. The magnetic field fluctuations can be related to the amount of ferromagnetic martensitic material in the strain sensing element and thus to the amount of strain experienced by the rotating component.

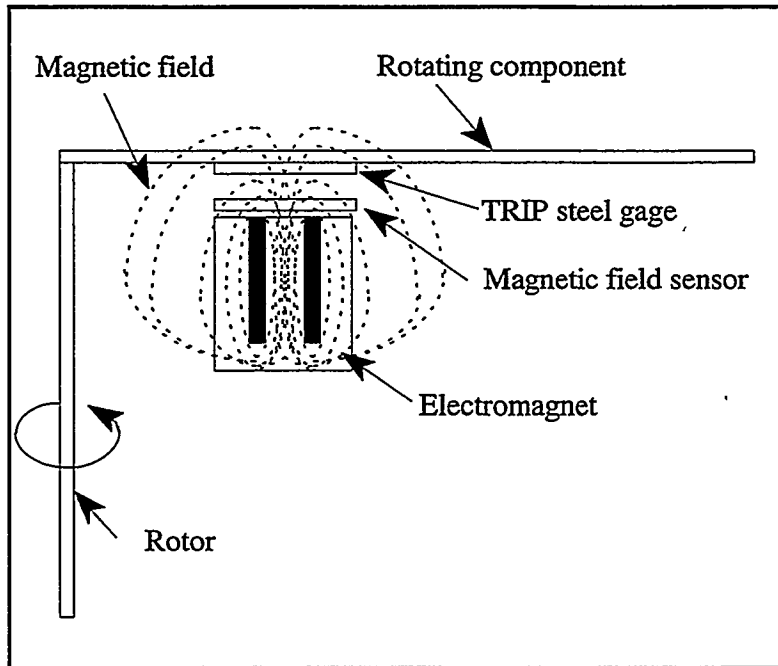


Fig. 1. A typical application of a TRIP steel sensor to measure strain in a rotating component.

The feasibility of the technique was investigated by applying the ElectroMagnetic Analysis System (EMAS) computer code, developed and distributed by the MacNeal-Schwendler Corporation, to calculate the magnetic fields near the magnetic coil.⁴ The effect on the magnetic field caused by variations in the magnetic properties of the TRIP steel strain sensor, the gap between the coil and the strain sensor, and the rotation speed were examined. A description of the EMAS model and the parametric study is presented in Sect. 2. Section 3 presents the calculation results, and conclusions and recommendations are presented in Sect. 4.

2. FINITE ELEMENT MODEL AND PARAMETRIC STUDY DESCRIPTION

The finite element models used to investigate the magnetic flux perturbations caused by the strain-induced phase transformation in the TRIP steel strain sensing element are described in this section. Axisymmetric, two-dimensional (2-D) static, and 2-D transient models were used in the analysis. The axisymmetric models were used to calculate the 3-D magnetic flux density when the TRIP steel strain sensor (which was modeled as a 0.635-mm-thick disk) was centered over the magnet. These results were used as the base analysis results. The 3-D magnetic flux and the 2-D magnetic flux are expected to be affected in quantitatively similar ways by motion-induced eddy currents. Thus, by comparing the calculated magnetic flux densities for the 2-D static and 2-D transient models, the effect on the 3-D magnetic flux could be estimated. A 3-D transient model could not be run to verify the validity of this assumption because of a lack of computer resources.

The finite element model is shown in Fig. 2. The model was created by meshing a cross section of the 3-D geometrical model of the system. The model is composed of an electrical steel armature, a coil, the TRIP steel disk, and a cylindrical volume of surrounding air. The magnetic material properties used in the model are listed in Appendix A. The magnetic flux was constrained to be tangent to the outer surface of the air region, and a steady-state excitation was applied to the coil regions to account for current flow through the coil. The coil excitation equals the total current

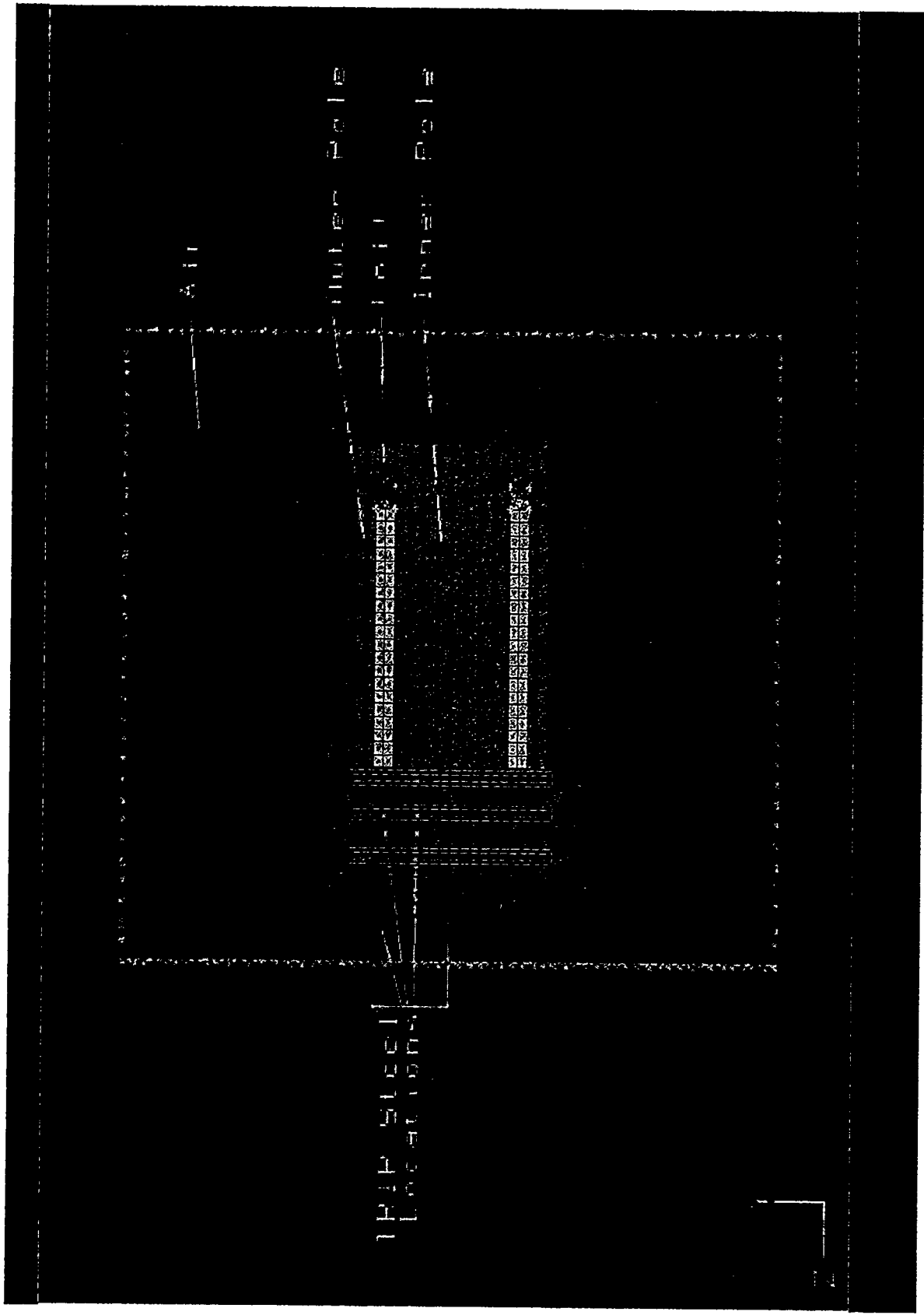


Fig. 2. The finite element model.

flowing out of the cross-sectional area of the coil, which is calculated by multiplying the number of coil turns by the coil current. The value used for the coil excitation, C_{cs} , is given by

$$C_{cs} = \frac{0.785 A_c A_{max}}{A_w}, \quad (1)$$

where

- A_c = total coil cross-sectional area,
- A_w = cross-sectional area of the wire,
- A_{max} = maximum current capacity of the wire,
- 0.785 = coil space factor for round wires.⁵

Assuming AWG #17 wire (diameter = 1.23 mm, $A_{max} = 2$ A), the maximum value for C_{cs} is 700 A. A value of 650 A was used in the analysis.

Additional structural constraints and initial conditions were needed for the transient models. All nodes were constrained to be fixed in the x and z directions. The rotation of all nodes in the three coordinate directions was also constrained. All nodes except those on the TRIP steel disk and nodes comprising the elements of air surrounding the TRIP steel disk were also constrained in the y direction. This combination of constraints allowed the TRIP steel disk to move in the y direction and the air elements surrounding the disk to deform as a result of the motion. An initial velocity and an initial displacement equal to the distance the disk would move over the analysis time were specified for the nodes comprising the TRIP steel disk. These initial conditions resulted in the centers of the disk and the magnet coinciding during the final time step. The magnetic flux density of the corresponding magnetostatic case was used as the electromagnetic initial condition.

Quadratic quadrilateral elements were used in the axisymmetric models, and linear quadrilateral elements were used in the 2-D static and transient models. Quadratic elements are preferable to linear elements because they give more accurate results for the same number of elements. However, limitations inherent in the EMAS code prevented quadratic elements from being used in the transient models; because the 2-D transient model used the 2-D static model results as initial conditions, linear elements were also used in the 2-D static models. The regions with the greatest mesh density, the TRIP steel disk regions and the bottom of the coil region, were meshed first. The steel armature was meshed next, and the air region was meshed last. After placing the electromagnetic boundary conditions and excitations on the model, an input file for EMAS was created.

If an input file for a transient model was being created, the initial EMAS input file was modified to include the structural constraints, the transient calculation control information (start time, end time, and time step), and the initial electromagnetic and structural conditions. The resulting file was then ready to be used to calculate a coupled electromagnetic/structural transient solution.

The parametric study examined the effects of air gap, TRIP steel element magnetic properties, and TRIP steel disk speed on the magnetic flux density. Air gaps of 2.54, 12.7, and 25.4 mm were used in this study. The TRIP steel magnetic properties, which were provided for 100% strained material, were modified to simulate the properties of lower strain. The B values for reduced strain cases were calculated by multiplying the 100% strained TRIP steel B values by the strain level for low values of H . At large values of H (i.e., for values of H beyond the “knee” of the B - H curve),

the B-H curves were given a slope of μ_0 . This practice makes the modified B-H curves conform to those provided by the MacNeal-Schwendler Corporation and results in more rapid convergence of the numerical solution. However, solutions containing flux densities greater than that corresponding to the "knee" of B-H curves modified in this way must be discarded. The resulting B-H curves are shown in Fig. 3. Strain levels of 10%, 25%, 50%, 75%, and 100% were used in the analysis. In the transient cases, TRIP steel disk velocities of 2.54, 12.7, and 25.4 m/s were used.

The axisymmetric magnetic flux calculated for the 100% strained TRIP steel disk located at 2.54 mm is shown in Fig. 4. The results show the magnetic flux confined primarily in the electrical steel armature, with flux concentrations at the corners of the coil slot and in the TRIP steel disk between the inner and outer magnet poles. The difference in the axisymmetric magnetic flux densities for a case with no TRIP steel and a case with 100% strained TRIP steel located at 2.54 mm is shown in Fig. 5. Figure 5 shows the spatial perturbation in magnetic flux caused by the TRIP steel disk. These results show that the optimum location for the flux density instrumentation is on the front face of the magnet because this location experiences a larger flux perturbation than any other portion of the air region. Therefore, the magnetic flux density averaged over the face of the magnet inside the coil (i.e., the inner pole), B, will be used as the measure of magnetic flux when presenting the analysis results.

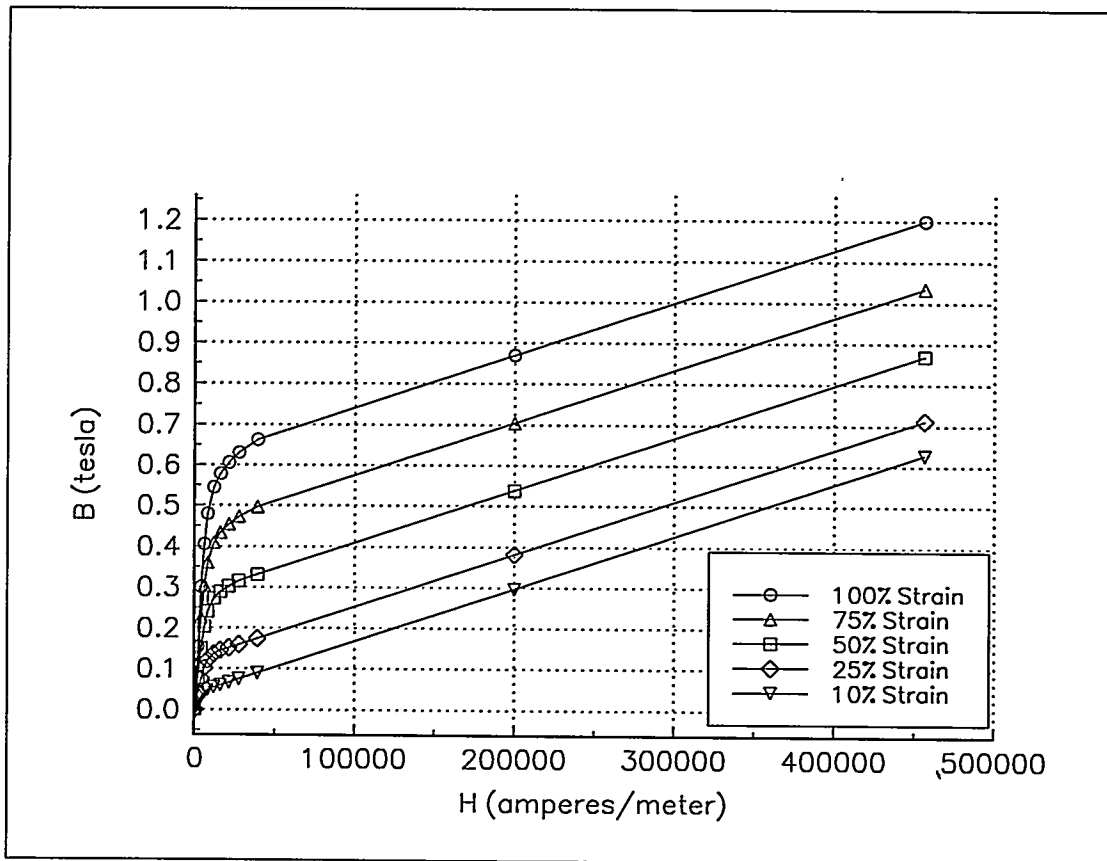


Fig. 3. B-H curves used in the analysis for TRIP steel.

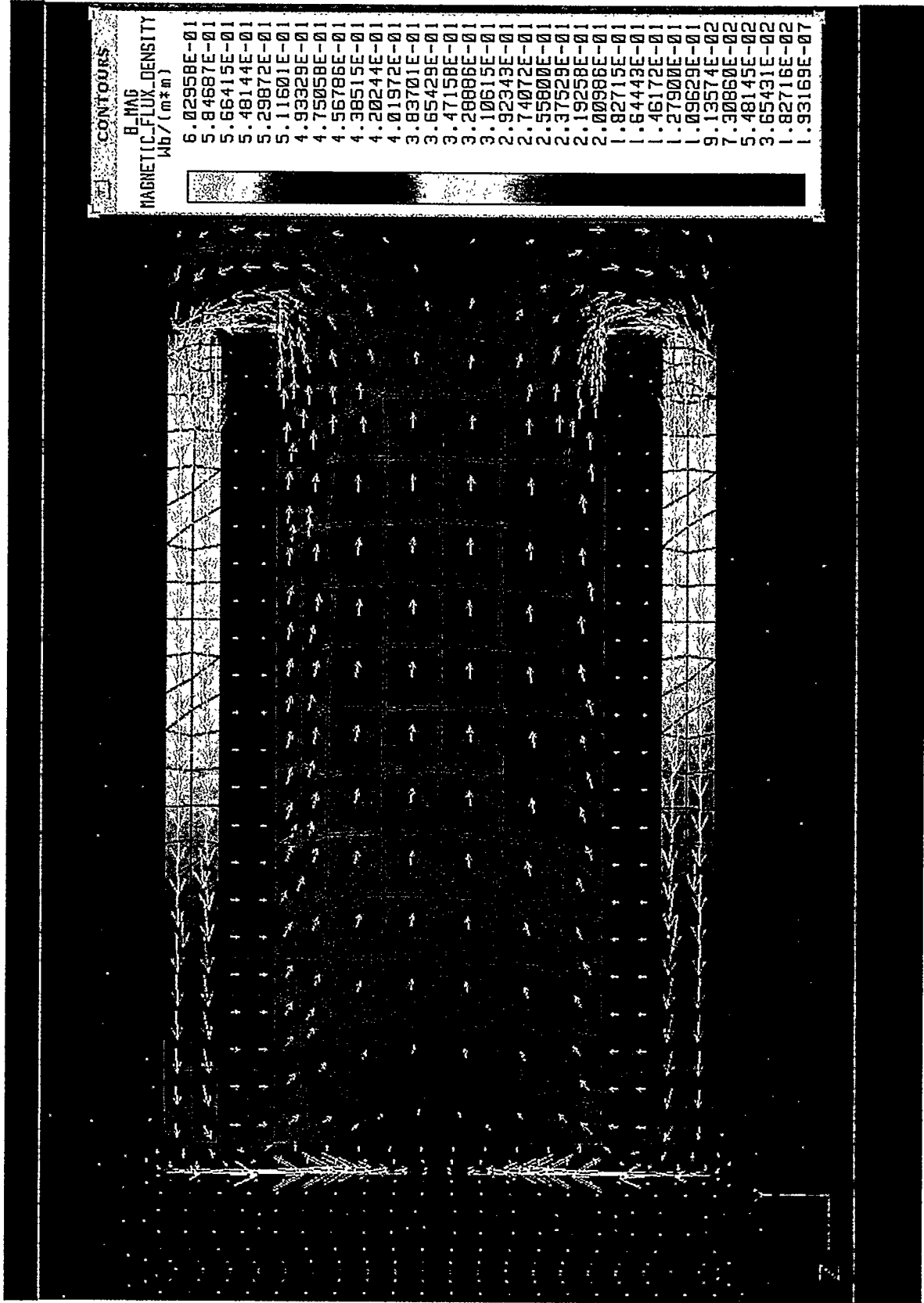
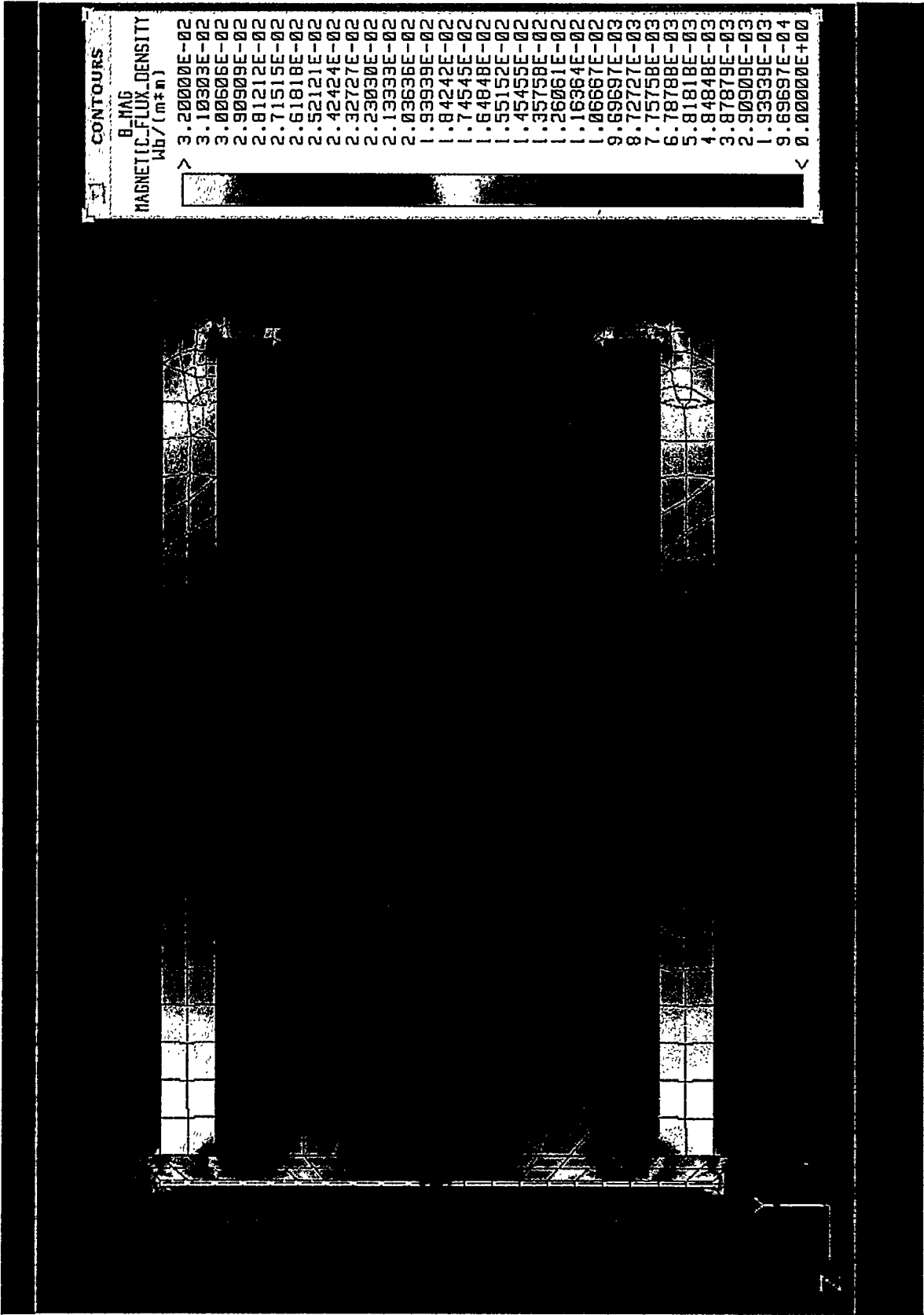


Fig. 4. Flux density for 100% strained TRIP steel with a 2.54-mm air gap.



CONTOURS

B_MAG
MAGNETIC_FLUX_DENSITY
Wb/(m²)

>

3.20000E-02
3.10000E-02
3.00000E-02
2.90000E-02
2.81212E-02
2.71515E-02
2.61818E-02
2.52121E-02
2.42424E-02
2.32727E-02
2.23030E-02
2.13333E-02
2.03636E-02
1.93939E-02
1.84242E-02
1.74545E-02
1.64848E-02
1.55152E-02
1.45455E-02
1.35758E-02
1.26061E-02
1.16364E-02
1.06667E-02
9.69697E-03
8.72727E-03
7.75758E-03
6.78788E-03
5.81818E-03
4.84848E-03
3.87879E-03
2.90909E-03
1.93939E-04
0.00000E+00

<

Fig. 5. Magnetic flux perturbation caused by the presence of 100% strained TRIP steel with a 2.54-mm air gap.

3. CALCULATION RESULTS

The results of the parametric study are presented in this section. The results for the axisymmetric static cases are presented first, followed by the results for the 2-D coupled electromagnetic/structural transient cases.

3.1 AXISYMMETRIC MAGNETOSTATIC RESULTS

The axisymmetric magnetic flux density averaged over the inner pole face, \bar{B} , for TRIP steel disk strains ranging from 0% to 100% and air gaps of 2.54, 12.7, and 25.4 mm is shown in Fig. 6 and listed in Table 1. The results show that \bar{B} is very sensitive to air gap and somewhat sensitive to TRIP steel strain level. Neglecting the effects of motion-induced eddy currents (which will be examined in the next section), the difference between each case and the all-air case is the maximum perturbation magnitude one would measure for the TRIP steel disk passing the stationary magnetic coil.

3.2 TWO-DIMENSIONAL MAGNETOSTATIC AND NONLINEAR TRANSIENT RESULTS

The 2-D model was used to examine the effects of motion-induced eddy currents on the magnetic flux density. The transient cases were given an initial velocity and an initial displacement such that during the final time step the TRIP steel elements were centered over the magnet. The calculated values of \bar{B} for initial velocities of 2.54, 12.7, and 25.4 m/s are shown for a 2.54-mm air gap in Fig. 7, for a 12.7-mm air gap in Fig. 8, and for a 25.4-mm air gap in Fig. 9. For each air gap, the effect of the initial velocity is negligible; the curves showing the average pole face flux density for different velocities are virtually indistinguishable from each other. This similarity is believed to be caused by the small thickness of the TRIP steel disk, by the magnetic flux density not being particularly large in the TRIP steel disk, and by the small rate of change in magnetic flux density over the range of motion examined in this study (i.e., near the centerline of the magnet).

Figure 10 shows the 2-D, zero velocity results calculated for the three different air gaps. Comparison of Figs. 6 and 10 shows qualitatively similar behavior; the flux density is highly dependent on the air gap thickness and somewhat less dependent on the TRIP steel strain level. The main conclusion that can be reached from the transient case results is that because the effect of motion-induced eddy currents is negligible, the axisymmetric results shown in Fig. 6 give an accurate indication of the magnetic flux perturbations caused by the presence of the TRIP steel disk.

4. CONCLUSIONS AND RECOMMENDATIONS

The calculated results indicate that the strain-induced change in TRIP steel disk properties can cause significant flux density perturbations as the disk passes the magnet face. The perturbation magnitude is affected by the air gap thickness and by the magnetic material properties of the TRIP

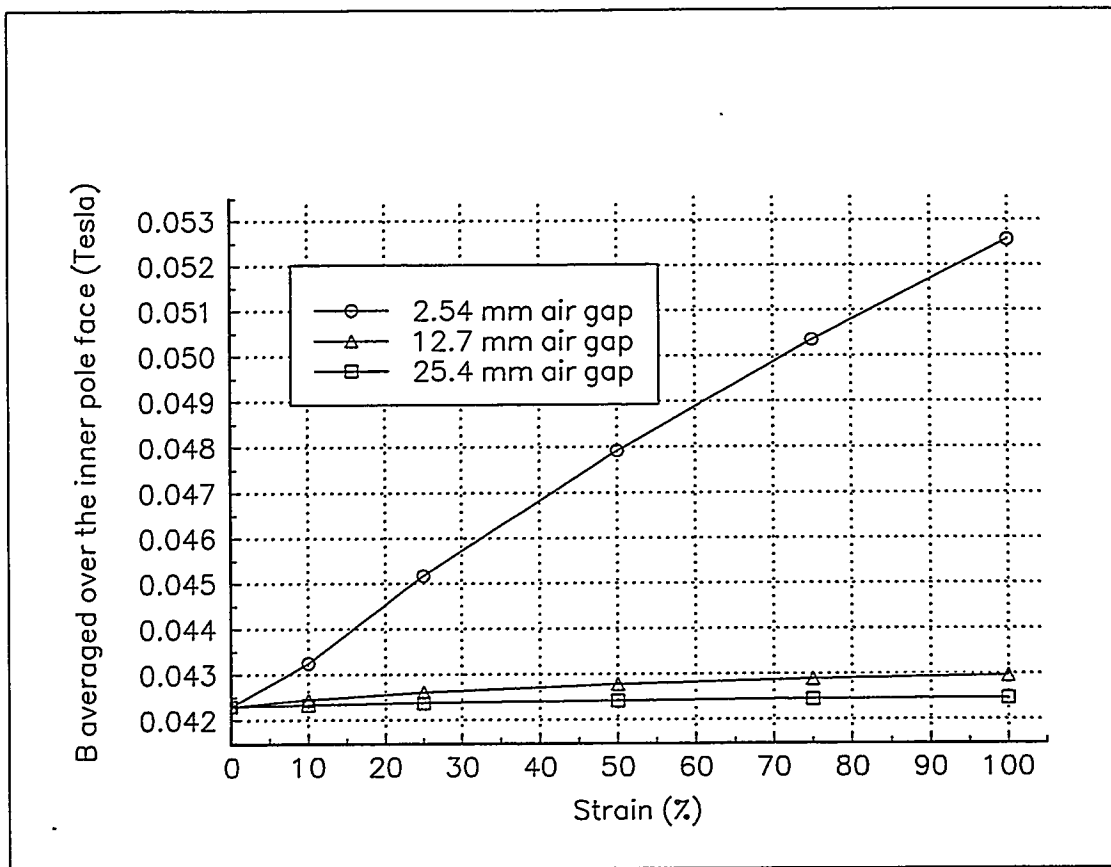


Fig. 6. Magnetic flux density averaged over the inner pole face for strain levels ranging from 0% to 100% and air gaps of 2.54, 12.7, and 25.4 mm.

Table 1. Effect of TRIP steel strain and air gap on average inner pole flux density

Strain level (%)	\bar{B} for 2.54-mm air gap (T)	\bar{B} for 12.7-mm air gap (T)	\bar{B} for 25.4-mm air gap (T)
0	0.0423	0.0423	0.0423
10	0.0432	0.0424	0.0423
25	0.0452	0.0426	0.0424
50	0.0479	0.0428	0.0424
75	0.0504	0.0429	0.0424
100	0.0525	0.0430	0.0425

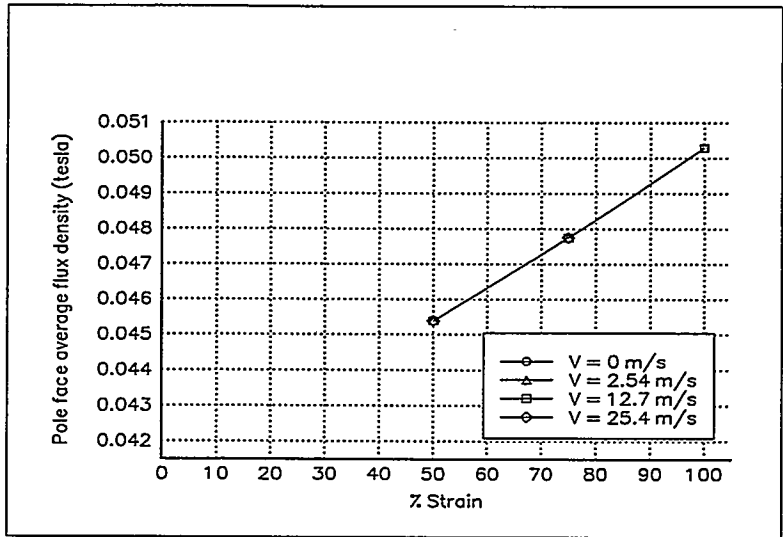


Fig. 7. Magnetic flux density averaged over the pole face for strain levels ranging from 50% to 100%; TRIP steel disk velocities of 0, 2.54, 12.7, and 25.4 m/s; and an air gap of 2.54 mm. The 10% and 25% cases are not shown because these cases failed to converge.

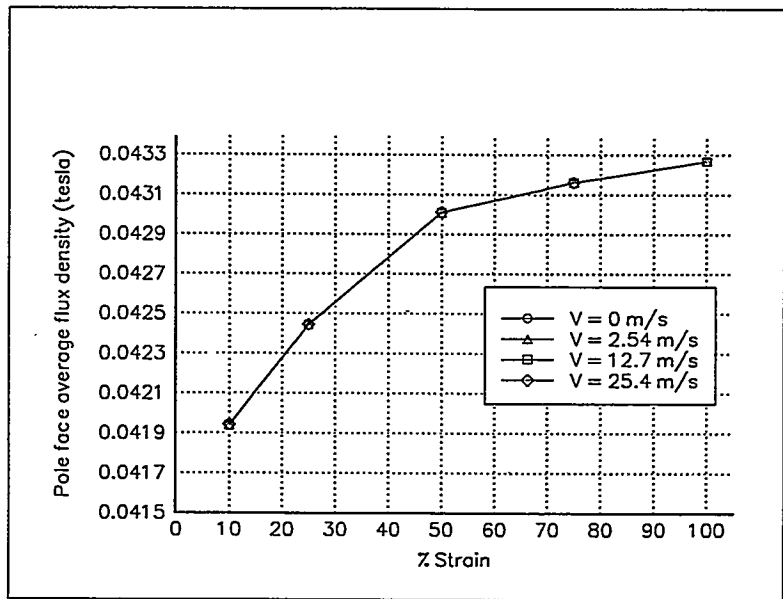


Fig. 8. Magnetic flux density averaged over the pole face for strain levels ranging from 10% to 100%; TRIP steel disk velocities of 0, 2.54, 12.7, and 25.4 m/s; and an air gap of 12.7 mm.

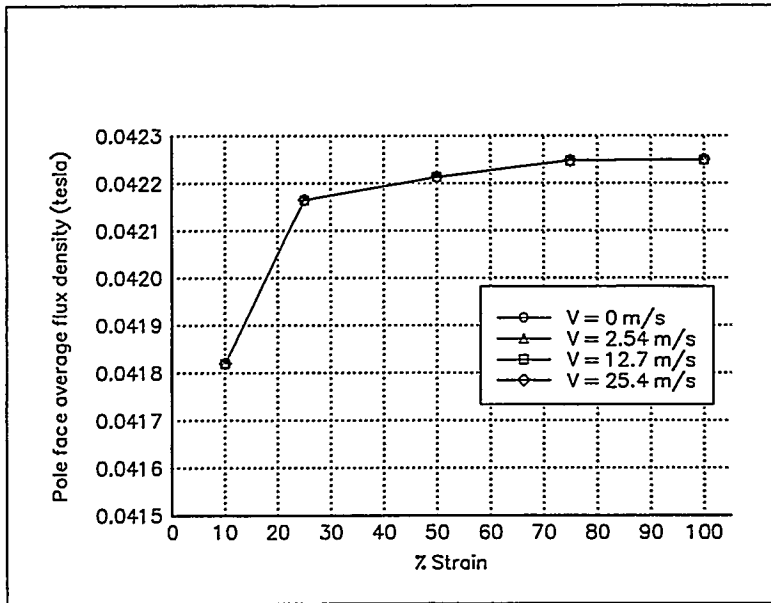


Fig. 9. Magnetic flux density averaged over the pole face for strain levels ranging from 10% to 100%; TRIP steel disk velocities of 0, 2.54, 12.7, and 25.4 m/s; and an air gap of 25.4 mm.

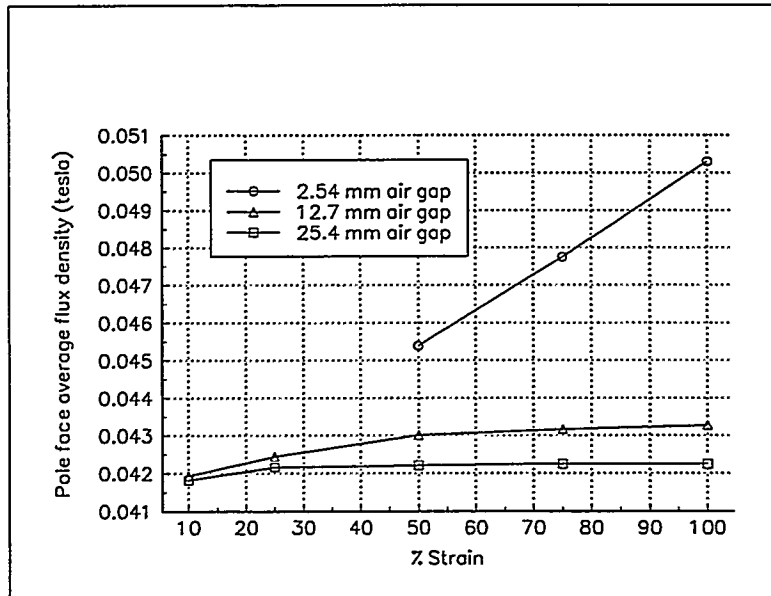


Fig. 10. Magnetic flux density averaged over the pole face for strain levels ranging from 10% to 100% and air gaps of 2.54, 12.7 and 25.4 mm.

steel disk; decreasing the air gap results in a greater sensitivity of the magnetic flux to TRIP steel disk material properties. Finally, it appears that the effect of motion-induced eddy currents on the magnetic flux density perturbations is negligible.

The calculated results suggest that strains in rotating components can be measured by using a TRIP steel gage bonded to the rotating part. The measurement will be most accurate for small air gaps (~6.4 mm or less) because the measurement sensitivity increases rapidly as the air gap thickness decreases. Thus the measurement could be made most easily on systems that allow small air gap thicknesses. Because of the rapid change in measurement sensitivity with air gap thickness, a system that can experience significant air gap thickness fluctuations will require an independent proximity measurement.

The negligible effect of motion-induced eddy currents on the flux density perturbations allows future analytical studies to be performed using simple axisymmetric or 2-D models. Thus, any future design or analysis work can be expected to be performed faster and may even be performed using smaller, less powerful analysis codes.

It is recommended that additional work be performed to produce a proof-of-principle demonstration of the noncontact strain measuring technique. A laboratory-scale demonstration would allow the effects of air gap thickness, TRIP steel strain level, and velocity to be verified. A proximity measurement could be incorporated into the system, and application pitfalls not apparent in the computer simulation could be exposed.

5. REFERENCES

1. *Nuclear News*, 37(7), 21 (May 1994).
2. V. F. Zackay, E. R. Parker, D. Fahr, and R. Busch, "The Enhancement of Ductility in High-Strength Steels," *Trans. Am. Soc. Metals*, 60, 252-259 (1967).
3. *A Damage Monitoring Technology for Safety Assessment of Structural Materials*, Report # 46-94, Strain Monitor Systems, Inc., San Diego, Calif., 1994.
4. J. R. Brauer, B. E. MacNeal, and J. C. Neuner, *MSC/EMAS Users Manual, Version 3*, The MacNeal-Schwendler Corporation, 815 Colorado Blvd., Los Angeles, CA 90041, 1994.
5. *Mark's Standard Handbook for Mechanical Engineers*, Eighth Edition, McGraw Hill Book Company, New York, 1978.

APPENDIX A

MAGNETIC MATERIAL PROPERTIES

The magnetic material properties used in the analysis are listed in this appendix. The material properties consist of the relative permeability, conductivity, relative permittivity, and B-H data for the TRIP steel and for the steel used in the magnet core. The TRIP steel B-H data were provided by Strain Monitor Systems, and the B-H data for the electrical steel used in the magnet core were supplied by the MacNeal-Schwendler Corporation as part of the EMAS/XL material properties library. Table A.1 lists the magnetic material properties used to model the air, coil, electrical steel, and TRIP steel. The B-H data for electrical steel are listed in Table A.2, and the B-H data for TRIP steel are given in Table A.3.

Table A.1. Magnetic material properties

Material	Relative permeability	Conductivity ($\Omega^{-1}\text{-m}^{-1}$)	Relative permittivity
Air	1.0	0.0	1.0
Coil	1.0	0.0	1.0
Steel		5.5×10^6	1.0
TRIP steel		5.5×10^6	1.0

Table A.2 B-H data for electrical steel

B (T)	H (A/m)	B (T)	H (A/m)
0.0	0.0	1.02×10^{-2}	8105
2.89×10^{-4}	230	1.26×10^{-2}	1.001×10^4
3.58×10^{-4}	285	1.65×10^{-2}	1.316×10^4
5.09×10^{-4}	405	2.16×10^{-2}	1.716×10^4
6.83×10^{-4}	544	2.67×10^{-2}	2.122×10^4
8.84×10^{-4}	704	3.30×10^{-2}	2.624×10^4
1.10×10^{-3}	878	4.24×10^{-2}	3.374×10^4
1.30×10^{-3}	1038	5.79×10^{-2}	4.604×10^4
1.60×10^{-3}	1272	8.05×10^{-2}	6.404×10^4
2.05×10^{-3}	1631	1.19×10^{-1}	9.486×10^4
2.62×10^{-3}	2081	1.72×10^{-1}	1.365×10^5
3.43×10^{-3}	2731	2.28×10^{-1}	1.816×10^5
4.32×10^{-3}	3444	3.59×10^{-1}	2.855×10^5
5.25×10^{-3}	4181	5.59×10^{-1}	4.447×10^5
6.36×10^{-3}	5060	7.59×10^{-1}	6.038×10^5
7.26×10^{-3}	5774	1.108	8.823×10^5
8.45×10^{-3}	6726		

Table A.3. B-H data for TRIP steel

H (A/m)	B 100% strain (T)	B 75% strain (T)	B 50% strain (T)	B 25% strain (T)	B 10% strain (T)
0.0	0	0	0	0	0
1990	0.155	0.116	0.078	0.039	0.0155
3979	0.300	0.225	0.150	0.075	0.0300
5969	0.405	0.304	0.203	0.101	0.0405
7958	0.480	0.360	0.240	0.120	0.0480
1.193×10^5	0.545	0.409	0.273	0.136	0.0545
1.592×10^5	0.578	0.434	0.289	0.145	0.0596
2.132×10^5	0.605	0.454	0.303	0.151	0.0666
2.757×10^5	0.630	0.473	0.315	0.159	0.0746
3.909×10^5	0.662	0.497	0.331	0.174	0.0895
2.000×10^5	0.869	0.704	0.538	0.382	0.297
4.565×10^5	1.200	1.035	0.869	0.712	0.627



INTERNAL DISTRIBUTION

- | | |
|---------------------|--------------------------------------|
| 1. D. J. Adams | 23. H. M. Meyer |
| 2. G. T. Alley | 24. G. N. Miller |
| 3. S. W. Allison | 25. T. P. Sjoreen |
| 4-13. B. Damiano | 26. J. O. Stiegler |
| 14. B. G. Eads | 27-31. L. J. Talarico |
| 15. R. G. Gilliland | 32. R. W. Tucker |
| 16. W. R. Hendrich | 33. R. E. Uhrig |
| 17. R. A. Hess | 34. J. D. White |
| 18. J. M. Jansen | 35. J. J. Yugo |
| 19. W. S. Key | 36. Central Research Library |
| 20. C. F. Leitten | 37. Y-12 Technical Reference Section |
| 21. D. W. McDonald | 38. Laboratory Records—Record Copy |
| 22. S. R. McNeany | 39. I&C Division Publications Office |

EXTERNAL DISTRIBUTION

40. P. E. Grayson, Strain Monitor Systems, Inc., 430 Tenth Street, NW, Suite N-102, Atlanta, GA 30318
41. B. D. Westermo, Strain Monitor Systems, Inc., 5151B Long Branch Ave., San Diego, CA 92107
42. P. E. Licato, The MacNeal-Schwendler Corporation, Electromagnetics Development Branch, 4300 Brown Deer Road, Suite 300, Milwaukee, WI 53223-2465
43. J. J. Burke, The MacNeal-Schwendler Corporation, Electromagnetics Development Branch, 4300 Brown Deer Road, Suite 300, Milwaukee, WI 53223-2465
44. Ron Moore, The RM Group, Inc., 12024 Broadwood Drive, Knoxville, TN 37922
45. David Norton, Houston Advanced Research Center, 4800 Research Forest Drive, The Woodlands, TX 77381
46. M. M. Sevik, Carderock Division, Naval Surface Warfare Center, Code 70, Bethesda, MD 20084-5000
47. Ernesto Suarez, Pratt & Whitney, P.O. Box 109600, Mail Stop 716-87, West Palm Beach, FL 33410-9600
- 48-49. Office of Scientific and Technical Information, U.S. Department of Energy, P.O. Box 62, Oak Ridge, TN 37831

